Transcriptomic profiling of *Streptococcus pyogenes* M1T1 strain in a mouse model of necrotizing fasciitis

Short title: *S. pyogenes* transcriptome in mouse necrotizing fasciitis model

Yujiro Hirose[1], Masaya Yamaguchi[1], Daisuke Okuzaki[2], Daisuke Motooka[2], Hiroshi Hamamoto[3], Tomoki Hanada[1], Tomoko Sumitomo[1], Masanobu Nakata[1], Shigetada Kawabata[1]*

1 Department of Oral and Molecular Microbiology, Osaka University Graduate School of Dentistry, Suita, Osaka 5650871, Japan

2 Genome Information Research Center, Research Institute for Microbial Diseases, Osaka University, Suita, Osaka 5650871, Japan

3 Institute of Medical Mycology, Teikyo University, Hachioji, Tokyo 1920352, Japan

*Corresponding author

E-mail: kawabata@dent.osaka-u.ac.jp (SK)

Keywords: *Streptococcus pyogenes*, necrotizing fasciitis, pathogenesis, RNA-sequencing

Abstract

Streptococcus pyogenes is a major cause of necrotizing fasciitis, a life-threatening subcutaneous soft-tissue infection. At the host infection site, the local environment and interaction between host and bacteria affect bacterial gene-expression profiles, but the *S. pyogenes* gene-expression pattern in necrotizing fasciitis remains unknown. In this study, we used a mouse model of necrotizing fasciitis and performed RNA-sequencing (RNA-seq) analysis of *S. pyogenes* M1T1 strain 5448 by using infected hindlimbs obtained at 24, 48, and 96 h post-infection. The RNA-seq analysis identified 483 bacterial genes whose expression was consistently altered in the infected hindlimbs as compared to their expression under *in vitro* conditions. The consistently enriched genes during infection included 306 genes encoding molecules involved in virulence, carbohydrate utilization, amino acid metabolism, trace-metal transport and vacuolar ATPase transport system. Surprisingly, drastic upregulation of 3 genes, encoding streptolysin S precursor (*sagA*), cysteine protease (*speB*), and secreted DNase (*spd*), was noted in the mouse model of necrotizing fasciitis ($\log_2$ fold-change values: >6.0, >9.4, and >7.1, respectively). Conversely, the consistently downregulated genes included 177 genes, containing genes associated with oxidative-stress response and cell division. These results suggest that *S. pyogenes* in necrotizing fasciitis changes its metabolism, decreases cell

38 proliferation, and upregulates the expression of major toxins. Our findings could provide
39 critical information for developing novel treatment strategies and vaccines for necrotizing
40 fasciitis. (218 words)
41

42 **Author summary**

43 Necrotizing fasciitis, a life-threatening subcutaneous soft-tissue infection, principally caused
44 by a *Streptococcus pyogenes*. At infection sites in hosts, bacterial pathogens are exposed to
45 drastically changing environmental conditions and alter global gene expression patterns for
46 survival and pathogenesis. However, there is no previous report about transcriptomic profiling
47 of *S. pyogenes* in the necrotizing fasciitis. Here, we conducted comprehensive gene-expression
48 analyses of *S. pyogenes* in the mouse model of necrotizing fasciitis at three distinct time points
49 during infection. Our results indicated that *S. pyogenes* drastically upregulates the expression
50 of virulence-associated genes and shifts metabolic-pathway usage during infection. The high-
51 level expressions in particular of toxins, such as cytolysins, proteases, and nucleases, were
52 observed at infection sites. In addition, the consistently enriched genes identified here included
53 genes for metabolism of arginine and histidine, and carbohydrate uptake and utilization.
54 Conversely, the genes associated with oxidative-stress response and cell division were
55 consistently downregulated in the mouse model of necrotizing fasciitis. These data will provide
56 useful information necessary for establishing novel treatment strategies (166 words).

57

Introduction

Streptococcus pyogenes causes diverse human diseases, ranging from mild throat and skin infections to life-threatening invasive diseases such as sepsis, necrotizing fasciitis, and streptococcal toxic-shock syndrome. Streptococcal necrotizing fasciitis cases are clinically characterized by fulminant tissue destruction and rapid disease progression [1]. In a majority of the cases, surgical treatment is required, including amputations, in addition to intensive care. Although this infection has been attracting increasing research and clinical interest, the mortality rate remains high [2, 3]. Investigation of the molecular pathogenesis of *S. pyogenes* in necrotizing fasciitis is expected to lead to the development of novel therapeutic strategies or effective treatments.

S. pyogenes typing has been historically conducted on the basis of antigenicity of M protein and T antigen (pilus major subunit). Currently, the sequence typing of the region encoding hypervariable region of M protein has been widely applied to classify this organism into at least 240 *emm* sequence types [4-6] and ~20 T serotypes [7, 8] have been identified. In industrialized societies, *S. pyogenes* serotype M1 (*emm* 1) isolates are considerably more common than other serotypes among invasive cases [6, 9-11], and the M1T1 clone in particular

74 is the most frequently isolated serotype from severe invasive human infections worldwide [12,
75 13].

76 At infection sites in hosts, bacterial pathogens are exposed to drastically changing
77 environmental conditions, which include the host cells, tissues, and immune response, as
78 compared to laboratory growth conditions. However, no previous report has compared *in vivo*
79 and *in vitro* transcriptome of *S. pyogenes*

80 Several comprehensive *in vitro* analyses of *S. pyogenes* gene expression performed using
81 microarray or RNA-sequencing (RNA-seq) approaches and revealed the roles of *S. pyogenes*
82 virulence-related regulators [14], such as CovRS [15, 16] and CcpA [17-19]. The transcriptome
83 profile of *S. pyogenes* from a mouse soft-tissue infection, which was obtained using microarray
84 analysis, indicated that *S. pyogenes* MGAS5005 (serotype M1) upregulated genes that are
85 involved in oxidative-stress protection and stress adaptation [20]. The results of another
86 microarray analysis on *S. pyogenes* MGAS5005 (serotype M1) demonstrated downregulation
87 of glycolysis genes and induction of genes involved in amino acid catabolism and of several
88 types of virulence genes in human blood [21]. These reports suggest that *S. pyogenes* changes
89 its expression levels of virulence factor and metabolic pathways to adapt to the host
90 environment.

Comprehensive understanding of bacterial transcriptomes *in vivo* will facilitate research aimed at developing therapeutic strategies or effective vaccine antigens. Although transposon-directed insertion-site sequencing using cynomolgus macaque model of necrotizing fasciitis was conducted recently [22], this method cannot assess the expression level of genes. In addition, transcriptome analysis of *S. pyogenes* in necrotizing fasciitis have not been performed to date. Here, we investigated the transcriptome profiling of *S. pyogenes* M1T1 strain 5448 by using a mouse model of necrotizing fasciitis, from the acute phase to the elimination phase, and we identified genes whose expression is consistently altered throughout the infection period. This new information may shed light on the development of novel therapeutic strategies for the infection.

Results

Establishing a technique for high-yield purification of bacterial RNA from mouse tissue

We used a mouse necrotizing fasciitis model as described previously, with minor modifications [23]. At 24 and 48 h after infection, the mouse model of necrotizing fasciitis was histologically similar to human necrotizing fasciitis in terms of tissue necrosis, the infection spread along the fascial planes, inflammatory-cell infiltration, hemorrhage and ulceration [24, 25] (Fig 1A and 1B). Extensive scab formation was detected at 48 h post-infection and elimination of pus from infected hindlimbs was observed at 96 h post-infection. At 96 h after infection, the weight of the mice tended to recover, and the bacterial burden at the infected site also decreased (S1 Fig). Therefore, we collected infected hindlimb samples from the 24, 48, and 96 h groups. To obtain bacterial RNA from infected tissues, we established a suitable protocol by using two types of beads (Fig 1C); this method allows us to remove most mouse RNA from samples and obtain high-yield purification of bacterial RNA (Fig 1D).

Similar gene-expression patterns of *S. pyogenes* at three distinct time points in infected hindlimbs

We performed RNA-seq analysis on *S. pyogenes* isolated from infected hindlimbs at 24, 48, and 96 h post-infection. RNA-seq data from *S. pyogenes* during the exponential growth phase in THY medium (Todd-Hewitt broth plus yeast extract) were defined as the control. To assess the global gene-expression profiles of the samples, we performed principal component analysis (PCA) (Fig 2A), hierarchical clustering analysis (S2 Fig), and k-means clustering (Fig 2B) by using the RNA-seq data. In PCA and hierarchical clustering analysis, bacterial RNA expression patterns of THY culture samples formed a cluster and the samples from the infected tissues were well separated. The 24 h_1 sample showed a global gene-expression profile that was distant from the profiles of other samples, whereas the heatmap of k-means clustering showed that the gene-expression profile of 24 h_1 was at least partially similar to that of samples from the infected tissues as indicated in Clusters A and B. The k-means clustering further suggested that most samples from infected hindlimbs show changes in global mRNA transcript patterns in opposite directions as compared to the THY group.

Consistently altered 483 bacterial genes at three time points in mouse necrotizing fasciitis model

Differentially expressed genes (DEGs; absolute $\log_2$ fold-change > 1 and adjusted P < 0.1) were detected between *S. pyogenes* in infected tissues and in THY broth (Fig 3A). In S1 Dataset, we provide the DEG details and list the following information for all the genes: gene ID, gene name, the gene-associated function, $\log_2$ fold-change, adjusted P value, and reads per kilobase per million mapped reads (RPKM) value. In comparisons of 48 h vs 24 h groups and 96 h vs 24 h groups, no DEGs were detected (Fig 3A), and only 4 DEGs were detected between 96 h and 48 h groups (S1 Dataset). These results indicate that *S. pyogenes* expresses similar genes at the three time points in the mouse model of necrotizing fasciitis. To identify the genes that are consistently enriched or downregulated in the mouse necrotizing fasciitis model, we drew Venn diagrams by using the DEGs from the comparisons of 24 h and THY groups, 48 h and THY groups, and 96 h and THY groups (Fig 3B); 28.0% of all 1,723 genes, 483 genes, were identified as consistently altered bacterial genes in infected hindlimbs (S2 Dataset). Among the 483 genes, 306 and 177 genes were upregulated and downregulated, respectively, at all three time points.

Marked upregulation of genes encoding virulence factors

149 The consistently enriched genes featured a high proportion of genes encoding virulence
150 factors, such as genes for cytolysins (*sagA-I*, *slo*), nucleases (*spd*, *spd3*, *sdaD2*), cysteine
151 protease (*speB*), factors involved in immune evasion (*endoS*, *spyCEP*, *scpA*, *sic*), superantigens
152 (*speA*, *smeZ*), and adhesins (*fbaA*, *lbp*, *emm*) (Table 1; S2 Dataset). Surprisingly, the RPKM
153 values of genes encoding streptolysin S precursor (*sagA*), *speB*, SpeB−inhibitor-encoding gene
154 (*spi*), and *spd* were extremely high and were consistently ranked within the top four (S1
155 Dataset; Fig 4). As compared with their expression under the THY condition, *sagA*, *speB*, *spi*,
156 and *spd* were expressed in mouse necrotizing fasciitis at the following levels (respectively):
157 $\log_2$ fold-change = >6.0, >9.3, >9.4, and >7.1. By contrast, the gene encoding macroglobulin-
158 binding protein (*grab*) was markedly downregulated at all three time points. Lastly, hyaluronic
159 acid synthesis operon (*hasABC*) was significantly upregulated in the 48 h and 96 h groups, but
160 no significant difference was detected in the 24 h group.

161 **Table 1. The expression levels of selected genes/operons/regulons.**

Gene category	SP5448 number	Gene name	Encoded function (s)	Log_2 fold change		
				24 h/THY	48 h/THY	96 h/THY
Virulence factors	870	*nga*	NAD glycohydrolase	5.05*	5.79*	5.49*
	880	*slo*	Pore forming cytoxin	4.80*	5.67*	5.35*
	1845	*endoS*	Immunoglobulin modifying protein	3.91*	5.10*	4.66*
	2470	*sda1*	Streptococcal nuclease D	4.08*	5.30*	4.93*
	3755	*spd3*	Streptococcal extracellular nuclease 3	5.11*	6.27*	5.70*
	4075	*grab*	Macroglobulin-binding protein	-4.11*	-5.43*	-5.32*
	1702	*speA*	Superantigen	1.11*	1.80*	2.23*
	6700-6740	*sagABCDEFHI*	Secreted cytotoxin	4.69*	5.76*	5.62*
	7800	*spyCEP*	IL-8 degrading protease	4.12*	5.37*	5.71*
	8645	*smeZ*	Superantigen	1.24*	1.20*	1.25*
	8690	*lbp*	Laminin-binding surface protein	6.56*	6.13*	7.04*
	8710-8730	*fbaA, scpA, sic, emm*	Mga virulence regulon	2.00*	2.94*	3.54*
	8800	*speB*	Strepotococcal cysteine protease	10.09*	9.38*	10.11*
	8820	*spd*	Streptococcal nuclease B	7.06*	7.80*	7.74*
	9365-9375	*hasABC*	Hyaluronic acid capsule biosynthesis	0.79	1.08*	1.39*
Carbohydrate utilization	1210-1240	*nanH*	Sialic acid production and catabolism	3.84*	3.84*	4.08*
	1830-1855	*pmi, scrK, endoS, scrAB*	Sucrose transport and catabolism	1.94*	3.12	2.23
	2540-2570	*lacABD*	Glactose transport and catabolism	3.53*	3.27*	3.83*
	4190-4210		Cellobiose transport	2.64*	3.47*	3.54*
	4275-4305	*malACDX, amyAB*	Cyclodextrin transport and catabolism	4.29*	6.23*	5.74*
	5660-5675	*ptsABCD*	Mannose/fructose/sorbose transport	2.67*	2.37*	2.84*
	8320-8350	*lacABDEFG, lacC.2*	Lactose transport and catabolism	2.95*	2.39*	3.81*
Amino acid utilization	3210-3235	*arcABCD,*	Arginine catabolism	5.88*	5.67*	5.84*
	8955-8995	*hutDGHIU, ftcD, fchA, fhs.2*	Histidine catabolism	6.38*	7.22*	7.27*
Peptide transport	1400-1420	*oppABCDF*	Oligopeptide transporter	0.69	0.88*	0.62
	8655-8675	*dppABCDF*	Dipeptide permease	1.79*	1.93*	2.78*
Oxidative stress response	3280	*dpr*	DNA protection during starvation protein	-0.86	-0.44	-1.19
	3875	*sodA*	Superoxide dismutase	-2.58*	-2.07*	-3.12*
	7040	*gpoA*	Glutathione peroxidase	-1.40*	-1.32*	-1.19*
	8945	*ahpC*	Alkyl hydroperoxide reductase	-0.64	-0.33	0.31
Trace metals transport	560-570	*adcRCB*	Zinc transport	1.86*	1.87*	2.29*
	1895-1920	*shr/shp/siaABCD*	Iron and manganese transport	3.73*	4.11*	4.29*
	2520-2530	*copZAY*	Copper transport	1.18*	0.23	1.93*
	7665-7675	*mtsABC*	Iron and manganese transport	0.56	0.72	0.18
	7885-7900	*fhuGBDA*	Iron and manganese transport	1.97*	2.06*	1.64*
	8685-8690	*htpA, lbp*	Zinc transport	6.48*	6.14*	6.97*
Sodium and protons transport	805-840	*ntpABCDEFKI*	V1-V0 (V)-ATPase transport system	3.11*	4.49*	4.67*
	6640-6675	*atpABCDEFGH*	F1-F0 (F)-ATPase transport system	-0.97	-1.14*	-1.38*

162

163 Only the gene name annotated by PATRIC are represented.

164 Log_2 fold-changes of operons or regulons are mean log_2 fold-change in transcript level for all

165 genes.

166 Asterisks indicate significant difference, *P < 0.1.

167 In operons or regulons, asterisks indicated that significant difference was confirmed in all

168 included genes.

169 **Upregulation of carbohydrate uptake and utilization genes**

170 The consistently enriched genes also included most genes encoding ATP-binding cassette
171 (ABC) transporters or phosphoenolpyruvate-phosphotransferase system (PTS) molecules
172 responsible for carbohydrates transport (Fig 5; Table 1; S2 Dataset). In the glycolysis pathway,
173 the expression of *pgk* (encoding phosphoglycerate kinase) and *eno* (encoding enolase) showed
174 a slight decrease, but the RPKM values of these genes consistently remained at >1,500. Despite
175 the sufficient expression of glycolysis-system molecules in the infected hindlimbs, the
176 carbohydrate transport systems exhibited an overall increase. Shelburne *et al.* reported that the
177 carbon catabolite protein CcpA upregulates the expression of most operons encoding
178 transporters of carbohydrates, such as glucose, lactose, maltodextrin, mannose, fructose,
179 cellobiose, lactose, galactose, and sialic acid, under glucose-limiting conditions [18]. Moreover,
180 our results indicated that the genes encoding phosphocarrier protein (*ptsH*) and its kinase (*ptsK*)
181 were consistently downregulated (Fig 5). When Gram-positive bacteria are in the presence of
182 glucose, phosphocarrier protein (HPr) is phosphorylated at Ser46 by its kinase, HprK, which
183 allows phosphorylated HPr to dimerize with CcpA; the dimerized proteins then bind to
184 catabolite-response elements present in promoter sequences and elicit carbon catabolite

185 repression [26]. These findings raise the possibility that *S. pyogenes* is relieved from carbon
186 catabolite repression in the mouse model of necrotizing fasciitis.
187
188 **Drastically enhanced arginine and histidine metabolism in infected hindlimbs**
189 *S. pyogenes* is auxotrophic for at least 15 amino acids [27]. The consistently enriched genes
190 identified here included operons for metabolism of arginine (*arcABCD*), histidine (*hutDGHIU*,
191 *ftcD*,*fchA*,*fhs.2*), and serine (*salB*) (Table 1; Fig 4; Fig 6; S2 Dataset). Conversely, the bacterial
192 genes encoding proteins for isoleucine metabolism (*bcaT*, *acoC*) were consistently
193 downregulated in the infected hindlimbs (Fig 6). The operon for the dipeptide transporter
194 *dppABCDF*, which is involved in the uptake of essential amino acids [28], was also upregulated
195 in the infected hindlimbs (Table 1), and the expression of *dppA*, which encodes a dipeptide-
196 binding protein, was remarkably enhanced ($\log_2$ fold-change > 2.25) (Fig 4; S2 Dataset).
197 The mean fold-changes in the transcript levels (i.e., the mean $\log_2$ fold-change values) for
198 all genes in the operons for arginine and histidine metabolism were >5.67 and >6.38,
199 respectively. In *S. pyogenes*, the arginine deiminase pathway (*arcABCD*) is reported to
200 supplement energy production, help protect against acid stress, and compete with arginine-
201 dependent NO production by host cells in the subcutaneous layer [29]. Another critical role of

arginine metabolism is to serve as the source of uridine monophosphate (Fig 6A), whereas histidine metabolism is connected to the synthesis of inosine monophosphate (Fig 6B). These functions cooperate with pyrimidine and purine metabolism for the synthesis of DNA and RNA. The consistently enriched genes also included genes for pyrimidine and purine metabolism (S2 Dataset). These results suggest the possibility that bacterial synthesis of nucleic acids is active in infected hindlimbs, although we also observed the repression of certain genes related to cell division, such as genes encoding cell-division proteins (*ftsA*, *ftsZ*, *ftsH*), amino acid ligases (*murD*, *murG*), phospho-N-acetylmuramoyl-pentapeptide transferase (*mraY*), and ribonuclease III (*rnc*) (Fig 4; S1 and S2 Datasets).

Host-induced bacterial stress responses

Genes encoding superoxide dismutase (*sodA*) and glutathione peroxidase (*gpoA*) were consistently downregulated in the infected hindlimbs (Table 1; S2 Dataset). SodA and GpoA act to neutralize endogenous and exogenous peroxides, which contributes to detoxification of reactive oxygen species *in vitro* [30, 31]. Our results suggest that *S. pyogenes* is not exposed to substantial oxidative stress in the infected hindlimbs as compared to the stress encountered during the aerobic growth.

Transition metals are involved in several crucial biological processes in pathogens that are necessary for the pathogens to survive, proliferate, and cause diseases in their environmental niche. In *S. pyogenes*, contributions to virulence are made by the homeostasis of metals, including iron, manganese [32], and zinc [33], whereas hosts exploit this phenomenon and combat invading pathogens by restricting the availability of essential metals by using transferrin (iron), lactoferrin (iron), and calprotectin (manganese and zinc) [34]. Here, *S. pyogenes* was found to upregulate genes involved in iron and manganese transport (*shr/shp/siaABCD*, *fhuGBDA*) and zinc transport (*adcRCB*, *htpA*, *lbp*) in the mouse model of necrotizing fasciitis (Table 1; S2 Dataset).

Altered expression of virulence-related transcriptional-regulator genes

Expression of most virulence genes in *S. pyogenes* is under the control of two-component signal transduction systems (TCSs) and transcriptional activators/repressors [14]. Although phosphorylation is recognized as a key modification by which regulators exert regional transcriptional control [26, 35, 36], the alternation of regulator gene-expression levels could also influence the degree of regulation.

235 *S. pyogenes* showed altered expression of several genes encoding virulence-related
236 regulators (Fig 7): The consistently enriched genes included TCS *trxSR* operon and genes
237 encoding carbohydrate-sensitive regulators (*lacD.1*, *ccpA*), a member of the RofA-like protein
238 type family of stand-alone virulence-related regulators (*rivR/ralp4*), and maltose repressor
239 (*malR*). Conversely, the only consistently downregulated regulator gene was the gene encoding
240 streptococcal regulator of virulence (*srv*), although certain other regulators also tended to show
241 downregulation, including the genes for CovRS (*covRS*), the metabolic-control regulator
242 VicRK (*vicRK*), metalloregulator (*mtsR/scaR*), and RofA regulator (*rofA*).

Discussion

This is the first report of comprehensive gene-expression analyses of *S. pyogenes* in a mouse model of necrotizing fasciitis. For RNA-seq analysis of bacteria in host tissues, deep sequencing has been previously used to obtain a sufficient number of reads [37]. However, our protocol is simple and inexpensive and appears to effectively enable *in vivo* RNA-seq analysis of Gram-positive bacteria without deep sequencing. Here, we also analyzed the transcriptome profiles of *S. pyogenes* at three distinct time points during infection. Our results indicated that *S. pyogenes* drastically upregulates the expression of virulence-associated genes and shifts metabolic-pathway usage in the mouse model of necrotizing fasciitis consistently, and the results showed high-level expression in particular of *sagA*, *speB*, and *spd*. By contrast, *S. pyogenes* downregulated genes associated with oxidative-stress response and cell division in infected hind limbs relative to that in THY culture at the mid-logarithmic phase.

Our RNA-seq analysis revealed that *sagA*, *spi*, *speB* and *spd* were extremely upregulated in mouse necrotizing fasciitis as compared to in bacterial culture medium. Streptolysin S (SLS; encoded by *sagA-I*) and SpeB (encoded by *speB*) are widely recognized virulence factors of *S. pyogenes* [38]. SLS is involved in cellular injury, phagocytic resistance, and virulence in murine subcutaneous infection [39, 40], and SLS and SpeB promote *S. pyogenes* translocation

via a paracellular route by degrading epithelial junctions [41, 42]. SpeB is a secreted cysteine protease degrading a wide variety of host proteins including complement components and cytokines, and functions in escape of *S. pyogenes* from host immune response [43-47]. Moreover, SpeB has been shown to contribute its virulence substantially in mouse models of necrotizing myositis [23, 48]. The *spi* and *speB* genes are co-transcribed [49]. The *spi* gene encodes a specific SpeB inhibitor, Spi, to protect bacterial cell from the activity of residual unsecreted SpeB. We found that DNases encoded by *sda1*, *spd3*, and *spd* were also upregulated markedly. Sda1 allows *S. pyogenes* to escape killing in neutrophil extracellular traps and contributes to virulence in murine subcutaneous infection [50, 51]. The expression of *spd*, which encodes streptodornase B or mitogenic factor 1, was ranked 4th here, and a previous study has also reported its contribution to the virulence of *S. pyogenes* (serotype M89) [52]. Although *S. pyogenes* contains various virulence factors [12, 38, 53], these four genes showed outstanding up-regulation in our infection model. Our findings would help searching therapeutic targets for necrotizing facilities.

In this study, we also detected drastic upregulation of virulence genes encoding histidine triad protein (HtpA) [54] and laminin-binding protein (Lbp) [55]; our results could provide valuable insights regarding the utility of these molecules as therapeutic targets. Although we

277 used a mouse intraperitoneal-infection model, we found that HtpA functions as an effective
278 vaccine antigen against *S. pyogenes* [56]. Furthermore, analyses of sera from patients with
279 uncomplicated *S. pyogenes* infection or rheumatic fever indicated the detectable humoral
280 response against recombinant *S. pyogenes* Lbp [57].

281 The 483 genes that were consistently altered in this study overlap with the 150 low-
282 glucose-induced genes of strain HSC5 (serotype 14) [17]. The overlapping genes include the
283 upregulated genes encoding molecules involved in carbohydrate uptake and metabolism,
284 arginine metabolism, V-Type ATP synthase, and lactate oxidase, whereas the overlapping
285 downregulated genes contain molecules related to oxidative-stress response and cell division.
286 In terms of the expression of genes encoding virulence factors, we observed the overlapping of
287 upregulation of the genes for SLS, streptolysin O, and Spd and downregulation of GRAB gene.
288 These findings suggest that *S. pyogenes* in the infected hindlimbs encounters a glucose-poor
289 environment and relieves carbon catabolite repression [26].

290 Mutations in *covRS* of *S. pyogenes* serotype M1 (strains 5448) have been reported to
291 enhance virulence during subcutaneous infection in mouse and might be responsible for loss
292 of SpeB expression [51]. Graham *et al.* also reported that serotype M1 *S. pyogenes*
293 (MGAS5005) showed reduced levels of the *speB* transcript during growth in human blood [21].

294 However, in this study, the gene encoding SpeB was drastically upregulated in the mouse
295 model of necrotizing fasciitis ($\log_2$ fold-change > 9.38). The environment that *S. pyogenes*
296 encounters in necrotizing fasciitis is considered to be distinct from that in blood and in
297 subcutaneous tissue. Although blood pH is maintained in a narrow range around pH 7.4 in
298 living organisms, inflammatory loci are typically associated with an acidic environment [58].
299 Moreover, our results suggested that *S. pyogenes* encounters glucose deprivation in necrotizing
300 fasciitis. In *S. pyogenes*, *speB* expression at the early stationary phase can be substantially
301 suppressed by glucose and buffered pH [59]. Generally, the stationary phase of bacterial
302 growth is evidenced by glucose depletion and medium acidification. Thus, an environment
303 similar to the bacterial stationary phase might have induced the strong expression of *speB*.

304 Graham *et al.* also characterized the MGAS5005 (serotype M1) transcript profile in a
305 mouse soft-tissue infection model (subcutaneous infection) by using a wild-type strain and
306 Δ*covR* strain [20]; intriguingly, relative to the wild-type strain, Δ*covR* strain exhibited drastic
307 upregulation of *sagA* (18-fold), *speB* (2,053-fold), and *spd* (6-fold) in this model, and
308 normalized expression levels of these 3 genes ranked 8th, 2nd, and 5th, respectively, in Δ*covR*
309 strain. In our study, *S. pyogenes* in the mouse model of necrotizing fasciitis also showed
310 extremely high normalized expression levels of *sagA* (ranked 1st), *speB* (3rd), and *spd* (4th)

311 among 1723 genes. One of the classic signs of acute inflammation is heat, and muscle
312 temperature is considered to be higher than skin temperature [60]. *S. pyogenes* appears to
313 encounter higher temperatures during myositis than during subcutaneous infection, which
314 might lead to distinct transcriptome profiles of *S. pyogenes*.

315 Arginine and histidine are present in human muscle at high concentrations, ~1,000 and
316 500 μM, respectively [61]. Because a supply of amino acids is essential for protein and nucleic
317 acid synthesis, the arginine and histidine metabolic pathways are likely to be enhanced, as was
318 observed here, for pathogenicity to be exerted in necrotizing fasciitis. Moreover, for the uptake
319 of essential amino acids, the operon encoding dipeptide transporter (DppABCDF) was
320 consistently upregulated in the infected hindlimbs. Deletion of *S. pyogenes dppA* results in
321 *speB* expression decreasing to one-eighth of its original level (serotype M49, strain CS101)
322 [28]. Thus, *dppA* upregulation might contribute to the drastically increased expression of *speB*.

323 Recently, Zhu *et al.* identified the genes required for a cynomolgus macaque model of
324 necrotizing fasciitis by using transposon-directed insertion-site sequencing [22]. The serotype
325 M1 (MAGS2221) genes necessary for infection that were identified by Zhu *et al.* overlap with
326 certain upregulated genes in our study, such as genes for carbohydrate metabolism (*glgP*,
327 *malM*), arginine metabolism (*arcABCD*), and putative or known transporters (valine, *braB*;

328 zinc, *adcBC*; SLS, *sagGHI*). However, in transposon-directed insertion-site sequencing,
329 insertion sites are detected after DNA-sequencing, implying that gene-expression levels are not
330 considered. In RNA-seq analysis, relative expression levels among all genes can be evaluated.
331 For the investigation of therapeutic targets, it is critical to select highly expressed molecules,
332 which suggests the importance of our study for this purpose.

333 No transcriptome profiling of *S. pyogenes* in necrotizing fasciitis have been previously
334 reported. This study revealed that *S. pyogenes* in the mouse model of necrotizing fasciitis
335 exhibited substantially altered global transcription as compared to that under *in vitro* conditions.
336 *S. pyogenes* might have attempted to acquire nutrients by destroying tissues by markedly
337 upregulating the expression of toxins such as SLS, SpeB, and Spd. Furthermore, genes
338 encoding molecules involved in carbohydrate and amino acid utilization as well as metal-
339 transporter genes were upregulated in the infected mouse hindlimbs. We also believe that our
340 protocol for isolating bacterial RNA from infected tissues at high concentrations will facilitate
341 studies involving global gene-expression analyses of bacteria in the *in vivo* host environment.
342 Future studies could explore new therapies based on bacterial kinetics *in vivo* by exploiting our
343 data or our methods. The accumulation of *in vivo* gene-expression profiles will provide useful

344 information necessary for establishing novel treatment strategies or identifying effective

345 vaccine antigens.

346 **Materials and methods**

347 **Ethic statement**

348 All mouse experiments were conducted in accordance with animal protocols approved by
349 the Animal Care and Use Committee of Osaka University Graduate School of Dentistry (28-
350 002-0). Animals were cared for according to Guidelines for Proper Conduct of Animal
351 Experiments (Science Council of Japan) and the policy laid down by the Animal Care and Use
352 Committee of Osaka University Graduate School of Dentistry.

353

354 **Bacterial strains and culture conditions.**

355 *S. pyogenes* M1T1 strain 5448 (accession: CP008776) was isolated from a patient with
356 toxic-shock syndrome and necrotizing fasciitis; the strain is genetically representative of a
357 globally disseminated clone associated with invasive *S. pyogenes* infections [62]. *S. pyogenes*
358 strain 5448 was cultured in Todd-Hewitt broth (BD Biosciences, San Jose, CA) supplemented
359 with 0.2% yeast extract (BD Biosciences) (THY) at 37°C. For growth measurements, overnight
360 cultures of *S. pyogenes* strain 5448 were back-diluted 1:50 into fresh THY and grown at 37°C;
361 growth was monitored by measuring the optical density at 600 nm (OD_{600}).

362

363 **Necrotizing fasciitis studies**

364 We used 10-week-old male C57BL/6J mice (Charles River Japan Inc., Kanagawa, Japan)
365 for the necrotizing fasciitis studies, as described previously [23]. After growing *S. pyogenes*
366 cultures until the mid-exponential phase (OD_{600} = ~0.5), THY was replaced with PBS and the
367 bacterial suspensions were stored in a refrigerator (−80°C). Viable cell counts of the
368 suspensions were determined by plating diluted samples on THY blood agar. Mice were shaved
369 and hair was removed through chemical depilation (Veet, Oxy Reckit Benckiser, Chartes,
370 France), and then the mice were inoculated intramuscularly in both sides of hindlimbs with 2
371 × 10^7 CFU suspended in 100 μL of PBS, prepared immediately before infection by diluting
372 frozen stocks.

373 Mice were euthanized at 24, 48, or 96 h after infection by means of lethal intraperitoneal
374 injection of sodium pentobarbital, and then the infected hindlimbs were collected. The left
375 hindlimbs were immediately placed in RNAlater (Qiagen, Valencia, CA) and stored at -80°C
376 until use in RNA isolation, whereas the right hindlimbs were fixed with formalin, embedded
377 in paraffin and sectioned, and stained with hematoxylin and eosin, as described previously [63].

378

379 **RNA isolation**

Thawed tissues were placed in lysing Matrix D microtubes containing 1.4-mm silica spheres (Qbiogene, Carlsbad, CA) with RLT lysis buffer (RNeasy Fibrous Tissue Mini Kit, Qiagen, Hilden, Germany) and homogenized at 6,500 rpm for 45 s by using a MagNA Lyser (Roche, Mannheim, Germany). The lysate was centrifuged, and the obtained pellet was resuspended in lysing Matrix B microtubes containing 0.1-mm silica spheres (Qbiogene) with the RLT lysis buffer and homogenized at 6,500 rpm for 60 s by using the MagNA Lyser. The final lysate was centrifuged, and bacterial RNA was isolated from the collected supernatant by using the RNeasy Fibrous Tissue Mini Kit according to the manufacturer's guidelines and stored at -80°C (Fig 1B).

RNA-seq and data analysis

RNA integrity was assessed using a 2100 Bioanalyzer (Agilent Technologies, Santa Clara, CA) (Fig 1C). For RNA-seq, 5 μg of bacterial RNA was treated for ribosomal RNA (rRNA) removal by using a Ribo-Zero rRNA Removal Kit (Mouse and Bacteria) (Illumina Inc., San Diego, CA). Directional RNA-seq libraries were created using TruSeq RNA Sample Prep Kit v2 (Illumina Inc.), according to the manufacturer's recommendations. Libraries were sequenced using Illumina NovaSeq 6000 and HiSeq 2500 systems, with 100-bp paired-end

397 reads being obtained (Macrogen, Daejeon, Korea). Data were generated in the standard Sanger
398 FastQ format and raw reads were deposited into the DDBJ sequence read archive (DRA,
399 accession number: DRA008246). Phred-type quality scores Q30 were used for quality
400 trimming. RNA-seq reads were mapped against the *S. pyogenes* strain 5448 genome (accession
401 CP008776) by using the commercially available CLC Genomics workbench (version 9.5.2,
402 CLC Bio, Aarhus, Denmark). Differential expression analyses and global analysis of the RNA-
403 seq expression data were performed using iDEP (http://ge-lab.org/idep/) [64], with the RPKM
404 value of each sample being determined. Results were visualized using volcano plots (iDEP)
405 and Venn diagrams (http://bioinformatics.psb.ugent.be/webtools/Venn/). EdgeR log-
406 transformation was used for clustering and PCA (iDEP). The hierarchical clustering was
407 illustrated by using the average-linkage method with correlation distance (iDEP). The data
408 were also clustered by using k-means with 1,723 genes (k = 4) (iDEP). We classified the DEGs
409 into functional categories based on the bacterial bioinformatics database and analysis resource
410 PATRIC (www.patricbrc.org) [65], which is integrated with information from VFDB
411 (http://www.mgc.ac.cn/VFs/) [66], Victors [67], subsystems technology toolkit (*RASTtk*) [68,
412 69], and KEGG map [70]. Genes were also classified into pathways based on BioCyc database
413 [71]. The transcriptomic (RNA-seq) data are summarized in S1 Dataset.

Acknowledgment

We acknowledge the NGS core facility of the Genome Information Research Center at the Research Institute for Microbial Diseases of Osaka University for the support in RNA sequencing and data analysis.

418 **References**

419 1. Stevens DL, Bryant AE. Severe Group A Streptococcal Infections. In: Ferretti JJ,
420 Stevens DL, Fischetti VA, editors. *Streptococcus pyogenes* : Basic Biology to Clinical
421 Manifestations. Oklahoma City (OK)2016.
422 2. Nelson GE, Pondo T, Toews KA, Farley MM, Lindegren ML, Lynfield R, et al.
423 Epidemiology of Invasive Group A Streptococcal Infections in the United States, 2005-
424 2012. Clin Infect Dis. 2016;63(4):478-86. doi: 10.1093/cid/ciw248. PMID: 27105747.
425 3. Misiakos EP, Bagias G, Patapis P, Sotiropoulos D, Kanavidis P, Machairas A. Current
426 concepts in the management of necrotizing fasciitis. Front Surg. 2014;1:36. doi:
427 10.3389/fsurg.2014.00036. PMID: 25593960.
428 4. Carapetis JR, Steer AC, Mulholland EK, Weber M. The global burden of group A
429 streptococcal diseases. Lancet Infect Dis. 2005;5(11):685-94. doi: 10.1016/S1473-
430 3099(05)70267-X. PMID: 16253886.
431 5. Sanderson-Smith M, De Oliveira DM, Guglielmini J, McMillan DJ, Vu T, Holien JK, et
432 al. A systematic and functional classification of *Streptococcus pyogenes* that serves as a
433 new tool for molecular typing and vaccine development. J Infect Dis. 2014;210(8):1325-
434 38. doi: 10.1093/infdis/jiu260. PMID: 24799598.
435 6. Steer AC, Law I, Matatolu L, Beall BW, Carapetis JR. Global *emm* type distribution of
436 group A streptococci: systematic review and implications for vaccine development.
437 Lancet Infect Dis. 2009;9(10):611-6. doi: 10.1016/S1473-3099(09)70178-1. PMID:
438 19778763.
439 7. Mora M, Bensi G, Capo S, Falugi F, Zingaretti C, Manetti AG, et al. Group A
440 *Streptococcus* produce pilus-like structures containing protective antigens and Lancefield
441 T antigens. Proc Natl Acad Sci U S A. 2005;102(43):15641-6. doi:
442 10.1073/pnas.0507808102. PMID: 16223875.
443 8. Falugi F, Zingaretti C, Pinto V, Mariani M, Amodeo L, Manetti AG, et al. Sequence
444 variation in group A *Streptococcus* pili and association of pilus backbone types with
445 lancefield T serotypes. J Infect Dis. 2008;198(12):1834-41. doi: 10.1086/593176. PMID:
446 18928376.
447 9. Ekelund K, Darenberg J, Norrby-Teglund A, Hoffmann S, Bang D, Skinhoj P, et al.
448 Variations in *emm* type among group A streptococcal isolates causing invasive or
449 noninvasive infections in a nationwide study. J Clin Microbiol. 2005;43(7):3101-9. doi:
450 10.1128/JCM.43.7.3101-3109.2005. PMID: 16000420.
451 10. Shea PR, Ewbank AL, Gonzalez-Lugo JH, Martagon-Rosado AJ, Martinez-Gutierrez JC,
452 Rehman HA, et al. Group A *Streptococcus emm* gene types in pharyngeal isolates,

453 Ontario, Canada, 2002-2010. Emerg Infect Dis. 2011;17(11):2010-7. doi:
454 10.3201/eid1711.110159. PMID: 22099088.
455 11. Ikebe T, Tominaga K, Shima T, Okuno R, Kubota H, Ogata K, et al. Increased
456 prevalence of group A *streptococcus* isolates in streptococcal toxic shock syndrome
457 cases in Japan from 2010 to 2012. Epidemiol Infect. 2015;143(4):864-72. doi:
458 10.1017/S0950268814001265. PMID: 25703404.
459 12. Walker MJ, Barnett TC, McArthur JD, Cole JN, Gillen CM, Henningham A, et al.
460 Disease manifestations and pathogenic mechanisms of Group A *Streptococcus*. Clin
461 Microbiol Rev. 2014;27(2):264-301. doi: 10.1128/CMR.00101-13. PMID: 24696436.
462 13. Aziz RK, Kotb M. Rise and persistence of global M1T1 clone of *Streptococcus*
463 *pyogenes*. Emerg Infect Dis. 2008;14(10):1511-7. doi: 10.3201/eid1410.071660. PMID:
464 18826812.
465 14. Vega LA, Malke H, McIver KS. Virulence-Related Transcriptional Regulators of
466 *Streptococcus pyogenes*. In: Ferretti JJ, Stevens DL, Fischetti VA, editors. *Streptococcus*
467 *pyogenes* : Basic Biology to Clinical Manifestations. Oklahoma City (OK)2016.
468 15. Shelburne SA, Olsen RJ, Suber B, Sahasrabhojane P, Sumby P, Brennan RG, et al. A
469 combination of independent transcriptional regulators shapes bacterial virulence gene
470 expression during infection. PLoS Pathog. 2010;6(3):e1000817. doi:
471 10.1371/journal.ppat.1000817. PMID: 20333240.
472 16. Dalton TL, Collins JT, Barnett TC, Scott JR. RscA, a member of the MDR1 family of
473 transporters, is repressed by CovR and required for growth of *Streptococcus pyogenes*
474 under heat stress. J Bacteriol. 2006;188(1):77-85. doi: 10.1128/JB.188.1.77-85.2006.
475 PMID: 16352823.
476 17. Kietzman CC, Caparon MG. Distinct time-resolved roles for two catabolite-sensing
477 pathways during *Streptococcus pyogenes* infection. Infect Immun. 2011;79(2):812-21.
478 doi: 10.1128/IAI.01026-10. PMID: 21098101.
479 18. Shelburne SA, Keith D, Horstmann N, Sumby P, Davenport MT, Graviss EA, et al. A
480 direct link between carbohydrate utilization and virulence in the major human pathogen
481 group A *Streptococcus*. Proc Natl Acad Sci U S A. 2008;105(5):1698-703. doi:
482 10.1073/pnas.0711767105. PMID: 18230719.
483 19. Kinkel TL, McIver KS. CcpA-mediated repression of streptolysin S expression and
484 virulence in the group A *streptococcus*. Infect Immun. 2008;76(8):3451-63. doi:
485 10.1128/IAI.00343-08. PMID: 18490461.

20. Graham MR, Virtaneva K, Porcella SF, Gardner DJ, Long RD, Welty DM, et al. Analysis of the transcriptome of group A *Streptococcus* in mouse soft tissue infection. Am J Pathol. 2006;169(3):927-42. doi: 10.2353/ajpath.2006.060112. PMID: 16936267.
21. Graham MR, Virtaneva K, Porcella SF, Barry WT, Gowen BB, Johnson CR, et al. Group A *Streptococcus* transcriptome dynamics during growth in human blood reveals bacterial adaptive and survival strategies. Am J Pathol. 2005;166(2):455-65. doi: 10.1016/S0002-9440(10)62268-7. PMID: 15681829.
22. Zhu L, Olsen RJ, Beres SB, Eraso JM, Saavedra MO, Kubiak SL, et al. Gene fitness landscape of group A *streptococcus* during necrotizing myositis. J Clin Invest. 2019;129(2):887-901. doi: 10.1172/JCI124994. PMID: 30667377.
23. Olsen RJ, Sitkiewicz I, Ayeras AA, Gonulal VE, Cantu C, Beres SB, et al. Decreased necrotizing fasciitis capacity caused by a single nucleotide mutation that alters a multiple gene virulence axis. Proc Natl Acad Sci U S A. 2010;107(2):888-93. doi: 10.1073/pnas.0911811107. PMID: 20080771.
24. Olsen RJ, Musser JM. Molecular pathogenesis of necrotizing fasciitis. Annu Rev Pathol. 2010;5:1-31. doi: 10.1146/annurev-pathol-121808-102135. PMID: 19737105.
25. Keller N, Andreoni F, Reiber C, Luethi-Schaller H, Schuepbach RA, Moch H, et al. Human Streptococcal Necrotizing Fasciitis Histopathology Mirrored in a Murine Model. Am J Pathol. 2018;188(7):1517-23. doi: 10.1016/j.ajpath.2018.03.009. PMID: 29684366.
26. Deutscher J, Herro R, Bourand A, Mijakovic I, Poncet S. P-Ser-HPr--a link between carbon metabolism and the virulence of some pathogenic bacteria. Biochim Biophys Acta. 2005;1754(1-2):118-25. doi: 10.1016/j.bbapap.2005.07.029. PMID: 16182622.
27. Davies HC, Karush F, Rudd JH. Effect of Amino Acids on Steady-State Growth of a Group A Hemolytic *Streptococcus*. J Bacteriol. 1965;89:421-7. PMID: 14255710.
28. Podbielski A, Leonard BA. The group A streptococcal dipeptide permease (Dpp) is involved in the uptake of essential amino acids and affects the expression of cysteine protease. Mol Microbiol. 1998;28(6):1323-34. doi: 10.1046/j.1365-2958.1998.00898.x. PMID: 9680220.
29. Cusumano ZT, Watson ME, Jr., Caparon MG. *Streptococcus pyogenes* arginine and citrulline catabolism promotes infection and modulates innate immunity. Infect Immun. 2014;82(1):233-42. doi: 10.1128/IAI.00916-13. PMID: 24144727.
30. Brenot A, King KY, Caparon MG. The PerR regulon in peroxide resistance and virulence of *Streptococcus pyogenes*. Mol Microbiol. 2005;55(1):221-34. doi: 10.1111/j.1365-2958.2004.04370.x. PMID: 15612930.

31. King KY, Horenstein JA, Caparon MG. Aerotolerance and peroxide resistance in peroxidase and PerR mutants of *Streptococcus pyogenes*. J Bacteriol. 2000;182(19):5290-9. doi: 10.1128/JB.182.19.5290-5299.2000. PMID: 10986229.
32. Hanks TS, Liu M, McClure MJ, Fukumura M, Duffy A, Lei B. Differential regulation of iron- and manganese-specific MtsABC and heme-specific HtsABC transporters by the metalloregulator MtsR of group A *Streptococcus*. Infect Immun. 2006;74(9):5132-9. doi: 10.1128/IAI.00176-06. PMID: 16926405.
33. Weston BF, Brenot A, Caparon MG. The metal homeostasis protein, Lsp, of *Streptococcus pyogenes* is necessary for acquisition of zinc and virulence. Infect Immun. 2009;77(7):2840-8. doi: 10.1128/IAI.01299-08. PMID: 19398546.
34. Hood MI, Skaar EP. Nutritional immunity: transition metals at the pathogen-host interface. Nat Rev Microbiol. 2012;10(8):525-37. doi: 10.1038/nrmicro2836. PMID: 22796883.
35. Valdes KM, Sundar GS, Belew AT, Islam E, El-Sayed NM, Le Breton Y, et al. Glucose Levels Alter the Mga Virulence Regulon in the Group A *Streptococcus*. Sci Rep. 2018;8(1):4971. doi: 10.1038/s41598-018-23366-7. PMID: 29563558.
36. Churchward G. The two faces of Janus: virulence gene regulation by CovR/S in group A streptococci. Mol Microbiol. 2007;64(1):34-41. doi: 10.1111/j.1365-2958.2007.05649.x. PMID: 17376070.
37. Nuss AM, Beckstette M, Pimenova M, Schmühl C, Opitz W, Pisano F, et al. Tissue dual RNA-seq allows fast discovery of infection-specific functions and riboregulators shaping host-pathogen transcriptomes. Proc Natl Acad Sci U S A. 2017;114(5):E791-E800. doi: 10.1073/pnas.1613405114. PMID: 28096329.
38. Hamada S, Kawabata S, Nakagawa I. Molecular and genomic characterization of pathogenic traits of group A *Streptococcus pyogenes*. Proc Jpn Acad Ser B Phys Biol Sci. 2015;91(10):539-59. doi: 10.2183/pjab.91.539. PMID: 26666305.
39. Humar D, Datta V, Bast DJ, Beall B, De Azavedo JC, Nizet V. Streptolysin S and necrotising infections produced by group G *streptococcus*. Lancet. 2002;359(9301):124-9. doi: 10.1016/S0140-6736(02)07371-3. PMID: 11809255.
40. Datta V, Myskowski SM, Kwinn LA, Chiem DN, Varki N, Kansal RG, et al. Mutational analysis of the group A streptococcal operon encoding streptolysin S and its virulence role in invasive infection. Mol Microbiol. 2005;56(3):681-95. doi: 10.1111/j.1365-2958.2005.04583.x. PMID: 15819624.

554 41. Sumitomo T, Nakata M, Higashino M, Jin Y, Terao Y, Fujinaga Y, et al. Streptolysin S
555 contributes to group A streptococcal translocation across an epithelial barrier. J Biol
556 Chem. 2011;286(4):2750-61. doi: 10.1074/jbc.M110.171504. PMID: 21084306.
557 42. Sumitomo T, Mori Y, Nakamura Y, Honda-Ogawa M, Nakagawa S, Yamaguchi M, et
558 al. Streptococcal Cysteine Protease-Mediated Cleavage of Desmogleins Is Involved in
559 the Pathogenesis of Cutaneous Infection. Front Cell Infect Microbiol. 2018;8:10. doi:
560 10.3389/fcimb.2018.00010. PMID: 29416987.
561 43. von Pawel-Rammingen U, Björck L. IdeS and SpeB: immunoglobulin-degrading
562 cysteine proteinases of *Streptococcus pyogenes*. Curr Opin Microbiol. 2003;6(1):50-5.
563 doi: 10.1016/S1369-5274(03)00003-1. PMID: 12615219.
564 44. Honda-Ogawa M, Ogawa T, Terao Y, Sumitomo T, Nakata M, Ikebe K, et al. Cysteine
565 proteinase from *Streptococcus pyogenes* enables evasion of innate immunity via
566 degradation of complement factors. J Biol Chem. 2013;288(22):15854-64. doi:
567 10.1074/jbc.M113.469106. PMID: 23589297.
568 45. Terao Y, Mori Y, Yamaguchi M, Shimizu Y, Ooe K, Hamada S, et al. Group A
569 streptococcal cysteine protease degrades C3 (C3b) and contributes to evasion of innate
570 immunity. J Biol Chem. 2008;283(10):6253-60. doi: 10.1074/jbc.M704821200. PMID:
571 18160402.
572 46. Kapur V, Majesky MW, Li LL, Black RA, Musser JM. Cleavage of interleukin 1β (IL-
573 1β) precursor to produce active IL-1β by a conserved extracellular cysteine protease
574 from *Streptococcus pyogenes.* Proc Natl Acad Sci U S A. 1993;90(16):7676-80. doi:
575 10.1073/pnas.90.16.7676. PMID: 7689226.
576 47. Chiang-Ni C, Wu JJ. Effects of streptococcal pyrogenic exotoxin B on pathogenesis of
577 *Streptococcus pyogenes*. J Formos Med Assoc. 2008;107(9):677-85. doi:
578 10.1016/S0929-6646(08)60112-6. PMID: 18796357.
579 48. Do H, Makthal N, VanderWal AR, Rettel M, Savitski MM, Peschek N, et al. Leaderless
580 secreted peptide signaling molecule alters global gene expression and increases virulence
581 of a human bacterial pathogen. Proc Natl Acad Sci U S A. 2017;114(40):E8498-E507.
582 doi: 10.1073/pnas.1705972114. PMID: 28923955.
583 49. Kagawa TF, O'Toole P W, Cooney JC. SpeB-Spi: a novel protease-inhibitor pair from
584 *Streptococcus pyogenes*. Mol Microbiol. 2005;57(3):650-66. doi: 10.1111/j.1365-
585 2958.2005.04708.x. PMID: 16045611.
586 50. Buchanan JT, Simpson AJ, Aziz RK, Liu GY, Kristian SA, Kotb M, et al. DNase
587 expression allows the pathogen group A *Streptococcus* to escape killing in neutrophil

588 extracellular traps. Curr Biol. 2006;16(4):396-400. doi: 10.1016/j.cub.2005.12.039.
589 PMID: 16488874.
590 51. Walker MJ, Hollands A, Sanderson-Smith ML, Cole JN, Kirk JK, Henningham A, et al.
591 DNase Sda1 provides selection pressure for a switch to invasive group A streptococcal
592 infection. Nat Med. 2007;13(8):981-5. doi: 10.1038/nm1612. PMID: 17632528.
593 52. Sriskandan S, Unnikrishnan M, Krausz T, Cohen J. Mitogenic factor (MF) is the major
594 DNase of serotype M89 *Streptococcus pyogenes*. Microbiology. 2000;146 (Pt 11):2785-
595 92. doi: 10.1099/00221287-146-11-2785. PMID: 11065357.
596 53. Yamaguchi M, Terao Y, Kawabata S. Pleiotropic virulence factor - *Streptococcus*
597 *pyogenes* fibronectin-binding proteins. Cell Microbiol. 2013;15(4):503-11. doi:
598 10.1111/cmi.12083. PMID: 23190012.
599 54. Wen YT, Wang JS, Tsai SH, Chuan CN, Wu JJ, Liao PC. Label-free proteomic analysis
600 of environmental acidification-influenced *Streptococcus pyogenes* secretome reveals a
601 novel acid-induced protein histidine triad protein A (HtpA) involved in necrotizing
602 fasciitis. J Proteomics. 2014;109:90-103. doi: 10.1016/j.jprot.2014.06.026. PMID:
603 24998435.
604 55. Terao Y, Kawabata S, Kunitomo E, Nakagawa I, Hamada S. Novel laminin-binding
605 protein of *Streptococcus pyogenes*, Lbp, is involved in adhesion to epithelial cells. Infect
606 Immun. 2002;70(2):993-7. doi: 10.1128/IAI.70.2.993-997.2002. PMID: 11796638.
607 56. Kunitomo E, Terao Y, Okamoto S, Rikimaru T, Hamada S, Kawabata S. Molecular and
608 biological characterization of histidine triad protein in group A streptococci. Microbes
609 Infect. 2008;10(4):414-23. doi: 10.1016/j.micinf.2008.01.003. PMID: 18403236.
610 57. Wahid RM, Yoshinaga M, Nishi J, Maeno N, Sarantuya J, Ohkawa T, et al. Immune
611 response to a laminin-binding protein (Lmb) in group A streptococcal infection. Pediatr
612 Int. 2005;47(2):196-202. doi: 10.1111/j.1442-200x.2005.02038.x. PMID: 15771700.
613 58. Lardner A. The effects of extracellular pH on immune function. J Leukoc Biol.
614 2001;69(4):522-30. doi: 10.1189/jlb.69.4.522. PMID: 11310837.
615 59. Loughman JA, Caparon M. Regulation of SpeB in *Streptococcus pyogenes* by pH and
616 NaCl: a model for *in vivo* gene expression. J Bacteriol. 2006;188(2):399-408. doi:
617 10.1128/JB.188.2.399-408.2006. PMID: 16385029.
618 60. Costello JT, Culligan K, Selfe J, Donnelly AE. Muscle, skin and core temperature after -
619 110°C cold air and 8°C water treatment. PLoS One. 2012;7(11):e48190. doi:
620 10.1371/journal.pone.0048190. PMID: 23139763.
621 61. Canepa A, Filho JC, Gutierrez A, Carrea A, Forsberg AM, Nilsson E, et al. Free amino
622 acids in plasma, red blood cells, polymorphonuclear leukocytes, and muscle in normal

and uraemic children. Nephrol Dial Transplant. 2002;17(3):413-21. doi: 10.1093/ndt/17.3.413. PMID: 11865086.

62. Kansal RG, McGeer A, Low DE, Norrby-Teglund A, Kotb M. Inverse relation between disease severity and expression of the streptococcal cysteine protease, SpeB, among clonal M1T1 isolates recovered from invasive group A streptococcal infection cases. Infect Immun. 2000;68(11):6362-9. doi: 10.1128/IAI.68.11.6362-6369.2000. PMID: 11035746.
63. Hirose Y, Yamamoto T, Nakashima M, Funahashi Y, Matsukawa Y, Yamaguchi M, et al. Injection of Dental Pulp Stem Cells Promotes Healing of Damaged Bladder Tissue in a Rat Model of Chemically Induced Cystitis. Cell Transplant. 2016;25(3):425-36. doi: 10.3727/096368915X689523. PMID: 26395427.
64. Ge SX, Son EW, Yao R. iDEP: an integrated web application for differential expression and pathway analysis of RNA-Seq data. BMC Bioinformatics. 2018;19(1):534. doi: 10.1186/s12859-018-2486-6. PMID: 30567491.
65. Wattam AR, Davis JJ, Assaf R, Boisvert S, Brettin T, Bun C, et al. Improvements to PATRIC, the all-bacterial Bioinformatics Database and Analysis Resource Center. Nucleic Acids Res. 2017;45(D1):D535-D42. doi: 10.1093/nar/gkw1017. PMID: 27899627.
66. Liu B, Zheng D, Jin Q, Chen L, Yang J. VFDB 2019: a comparative pathogenomic platform with an interactive web interface. Nucleic Acids Res. 2019;47(D1):D687-D92. doi: 10.1093/nar/gky1080. PMID: 30395255.
67. Sayers S, Li L, Ong E, Deng S, Fu G, Lin Y, et al. Victors: a web-based knowledge base of virulence factors in human and animal pathogens. Nucleic Acids Res. 2019;47(D1):D693-D700. doi: 10.1093/nar/gky999. PMID: 30365026.
68. Aziz RK, Bartels D, Best AA, DeJongh M, Disz T, Edwards RA, et al. The RAST Server: rapid annotations using subsystems technology. BMC Genomics. 2008;9:75. doi: 10.1186/1471-2164-9-75. PMID: 18261238.
69. Brettin T, Davis JJ, Disz T, Edwards RA, Gerdes S, Olsen GJ, et al. RASTtk: a modular and extensible implementation of the RAST algorithm for building custom annotation pipelines and annotating batches of genomes. Sci Rep. 2015;5:8365. doi: 10.1038/srep08365. PMID: 25666585.
70. Kanehisa M, Sato Y, Kawashima M, Furumichi M, Tanabe M. KEGG as a reference resource for gene and protein annotation. Nucleic Acids Res. 2016;44(D1):D457-62. doi: 10.1093/nar/gkv1070. PMID: 26476454.

71. Caspi R, Altman T, Billington R, Dreher K, Foerster H, Fulcher CA, et al. The MetaCyc database of metabolic pathways and enzymes and the BioCyc collection of Pathway/Genome Databases. Nucleic Acids Res. 2014;42(Database issue):D459-71. doi: 10.1093/nar/gkt1103. PMID: 24225315.

662 **Figure legends**

663 **Fig 1. Features of a mouse model of necrotizing fasciitis and workflow of bacterial RNA**

664 **isolation.** (A) Representative images of infected hindlimbs after inoculation with *S. pyogenes*

665 M1T1 strain 5448. (B) Histopathological features of the mouse model of necrotizing fasciitis.

666 Hematoxylin and eosin staining of infected lesions at the indicated time points is shown, and

667 higher-magnification images of the selected areas of the same sections are presented. At 24 h

668 after infection, the skin shows erosion of the epidermis and edematous thickening of the dermis

669 (vertical bracket), as well as sparse inflammatory-cell infiltration. At 24 and 48 h after infection,

670 marked necrosis (asterisks) is observed, as is the presence of bacteria concentrated primarily

671 along the major fascial planes (arrows) in the infected deep soft tissue. At 96 h after infection,

672 sufficient inflammatory-cell infiltration and elimination of pus (red arrows) from infected

673 hindlimbs are observed. (C) Workflow of bacterial RNA isolation. At first, tissues were lysed

674 with 1.4-mm silica spheres and mouse RNA fraction was removed after centrifugation. Next,

675 pellets were lysed with 0.1-mm silica spheres and centrifuged to obtain bacterial RNA fraction.

676 (D) Representative bioanalyzer profile of total RNA isolated from an infected hindlimb; 16S

677 and 23S: bacterial rRNA peaks; 18S and 28S: mouse rRNA peaks.

678

679 **Fig 2. RNA-seq global reports.** (A) Principal component analysis (PCA) plot of RPKM data
680 from RNA-seq dataset. (B) Heatmap of k-means clustering of all genes (1,723 genes) in all
681 samples (k = 4). The number of expressed genes in each cluster is indicated. The color key
682 indicates Z-scores, which display the relative values of all tiles within all samples: green,
683 lowest expression; black, intermediate expression; red, highest expression. Bacterial RNA-seq
684 data at 24, 48, and 96 h post-infection were defined as 24-h group (24 h_1, 24 h_2, 24 h_3),
685 48-h group (48 h_1, 48 h_2, 48 h_3), and 96-h group (96 h_1, 96 h_2), respectively. Bacterial
686 RNA-seq data of THY culture samples were defined as the control and named THY group
687 (THY_1, THY_2, THY_3).

688

689 **Fig 3. Differentially expressed genes showing consistent alteration in hindlimbs at each**
690 **infection phase.** (A) Volcano plots showing gene-expression differences under the comparison
691 conditions indicated in each figure. Colored circles: significantly upregulated (red) and
692 downregulated (blue) genes (absolute $\log_2$ fold-change > 1; adjusted $P < 0.1$). (B) Three-way
693 Venn diagram illustrating bacterial genes that are consistently altered during infection (24 h vs
694 THY, 48 h vs THY, 96 h vs THY): relative to THY condition, 306 transcripts were consistently

695 enriched *in vivo* (log_2 fold-change > 1; adjusted P < 0.1) and 177 transcripts were consistently

696 downregulated *in vivo* (log_2 fold-change < −1; adjusted P < 0.1).

697

698 **Fig 4. Heatmap of significantly altered genes *in vivo*.** Heatmap of consistently and

699 significantly enriched genes (log_2 fold-change > 2, average RPKM *in vivo* > 1,000) or

700 downregulated genes (log_2 fold-change < -2, average RPKM in THY > 1,000); color scale

701 indicates enrichment (red) and depletion (blue) during infection. Values represent the log_2 fold-

702 change between indicated conditions, and genes are arranged in descending order of expression

703 level (average of RPKM values *in vivo*). AV RPKM, average RPKM.

704

705 **Fig 5. Central carbon metabolism and catabolite control protein CcpA.** The pathway

706 shown was constructed based on BioCyc database for *S. pyogenes* MGAS5005. Metabolite

707 names are written in black and gene names are written in red. The log_2 fold-changes of the 24-h

708 group (left), 48-h group (center), and 96-h group (right) with respect to THY group are

709 indicated in the color-scaled boxes. Color scale indicates enrichment (red) and depletion (blue)

710 during infection. Asterisks indicate significant difference: *P < 0.1. In operons or regulons,

711 asterisks indicate that significant difference was confirmed in all included genes. Log_2 fold-

712 change values of operons or regulons are mean $\log_2$ fold-changes in transcript levels for all
713 genes. The phosphocarrier protein HPr (*ptsH*) is phosphorylated at Ser46 by the kinase HPrK
714 (*ptsK*) through the cytoplasmic enzyme EI (*ptsI*), which allows HPr-Ser46-P to dimerize with
715 the carbon catabolite protein CcpA and elicit carbon catabolite repression by binding to
716 catabolite-response elements in promoter sequences [26].
717
718 **Fig 6. Significant enhancement of arginine and histidine metabolic pathways.** (A) Arginine
719 deiminase and pyrimidine nucleotide *de novo* synthesis pathways. (B) Histidine degradation
720 and purine nucleotide *de novo* biosynthesis pathways. (C) Glutamine, (D) isoleucine, (E) serine,
721 and (F) asparagine degradation pathways. Pathways were constructed based on BioCyc
722 database for *S. pyogenes* MGAS5005. Metabolite names are written in black and gene names
723 are written in red. The $\log_2$ fold-changes of 24-h group (left), 48-h group (center), and 96-h
724 group (right) with respect to THY group are indicated in color-scaled boxes. Color scale
725 indicates enrichment (red) and depletion (blue) during infection. Asterisks indicate significant
726 difference: *P < 0.1. UMP, uridine monophosphate; IMP, inosine monophosphate.
727

728 **Fig 7. Expression levels of genes encoding virulence-related transcriptional regulators.**

729 (A) Two-component signal transduction systems (TCSs) and (B) transcriptional regulators of

730 virulence. The $\log_2$ fold-changes of 24-h group (left), 48-h group (center), and 96-h group

731 (right) with respect to THY group are indicated in color-scaled boxes. Numbers in the frame

732 represent the measured $\log_2$ fold-change values. Color scale indicates enrichment (red) and

733 depletion (blue) during infection. Asterisks indicate significant difference: *P < 0.1.

734

Supporting information

S1 Fig. Mice recover from necrotizing fasciitis at 96 h after infection. Male C57BL/6J mice (10 weeks old) were intramuscularly inoculated in the hindlimbs with 2×10^7 CFU of *S. pyogenes*. (A) Body-weight change until sample collection. Body weight at 0 h was regarded as 100%. (B) CFU of *S. pyogenes* in infected hindlimb samples.

S2 Fig. Heatmap of clustering of all genes (1,723 genes) expressed in all samples. Each column represents a sample, and each row represents a gene. Clustering was performed by using iDEP (http://ge-lab.org/idep/) with edgeR log-transformation of reads per kilobase million (RPKM) values. The hierarchical clustering was illustrated by using the average-linkage method with correlation distance. Color-coding is based on edgeR log-transformed RPKM values. The color key indicates the Z-scores, which display the relative values of all tiles within all samples: green, lowest expression; black, intermediate expression; red, highest expression.

S1 Dataset. Global gene expression changes in a mouse model of necrotizing fasciitis.

S2 Dataset. Information of consistently altered mRNAs at three different distinct time-points during infection.

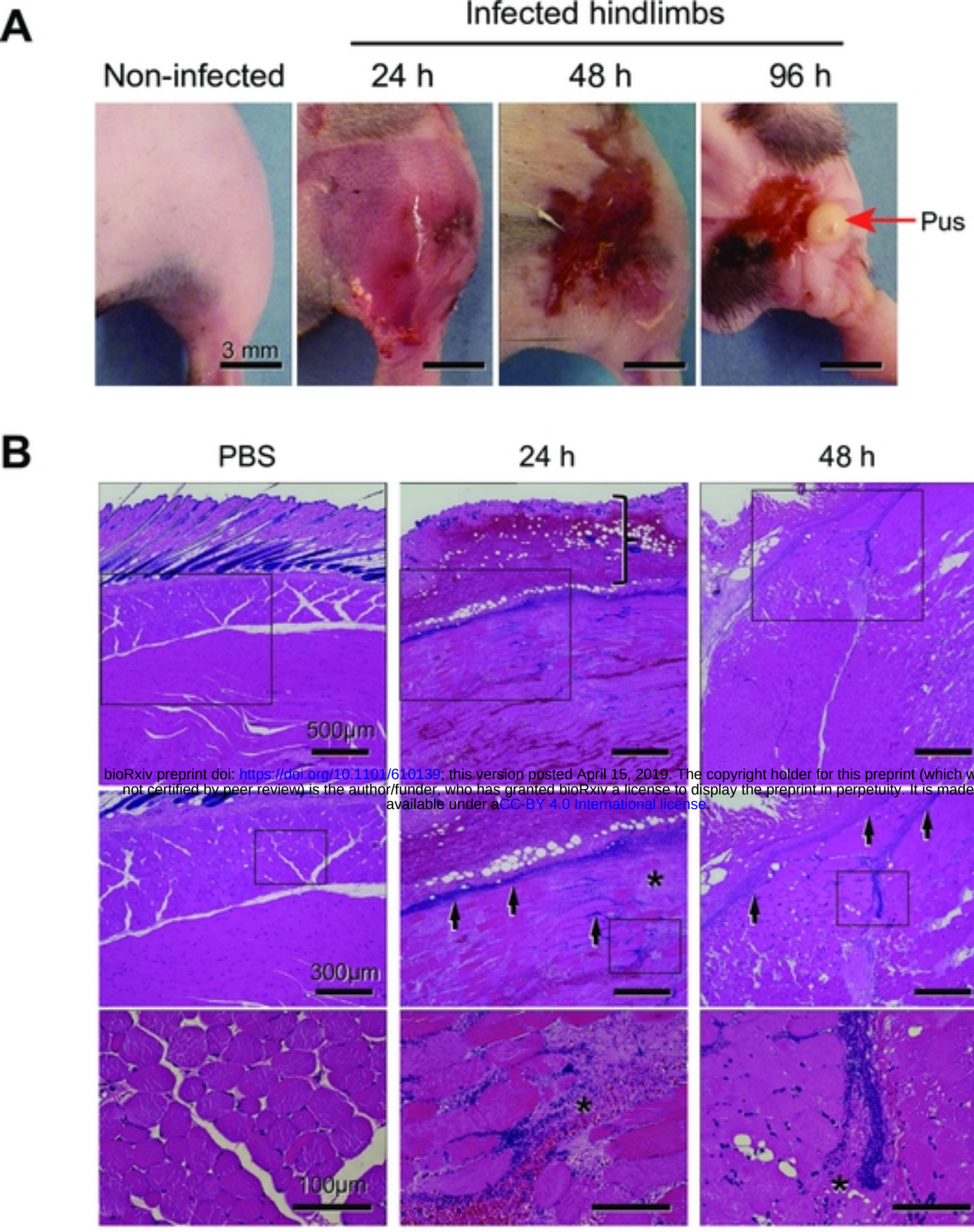

Figure 1. Hirose *et al.*

Figure 1

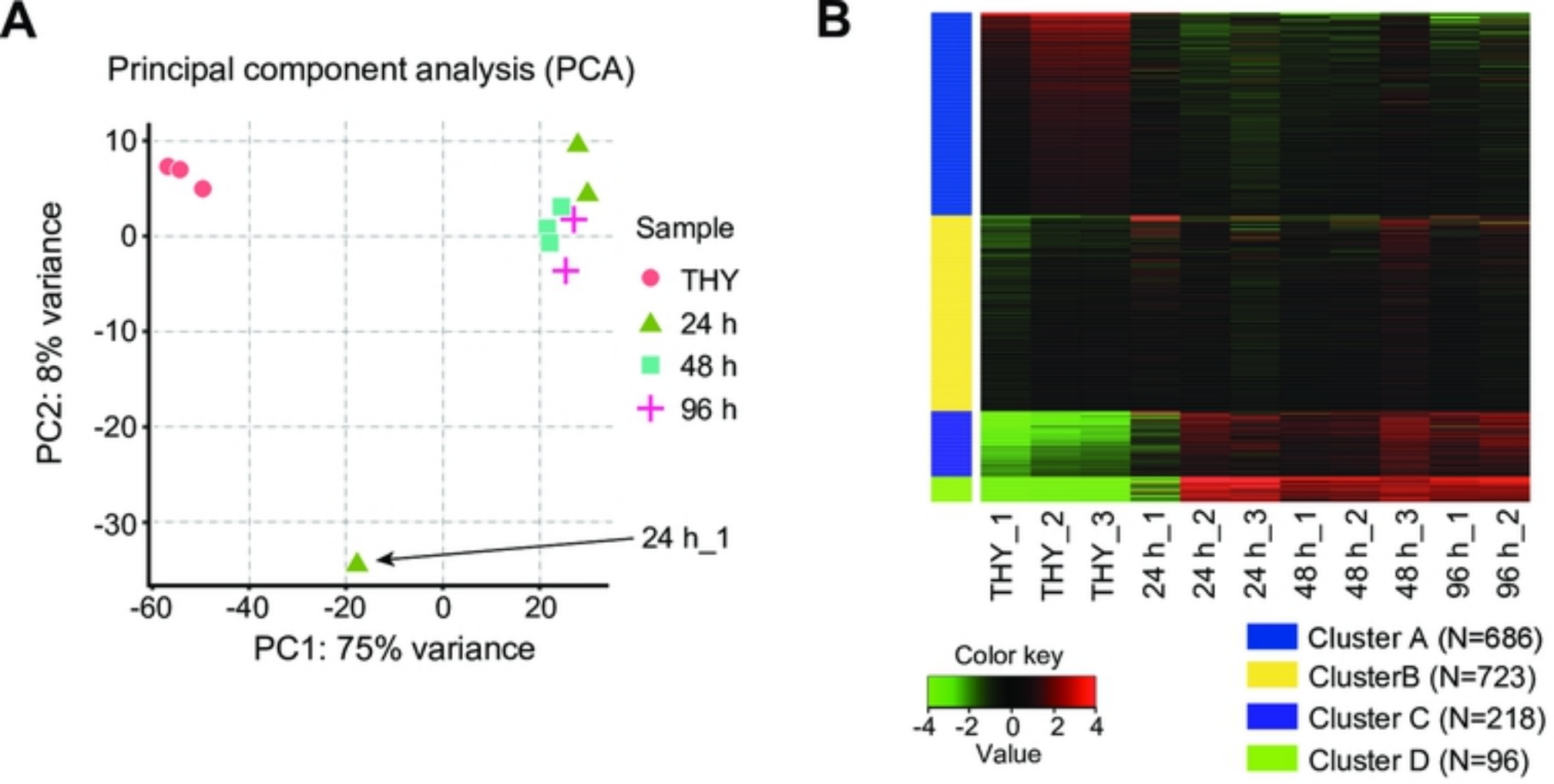

Figure 2. Hirose *et al.*

Figure 2

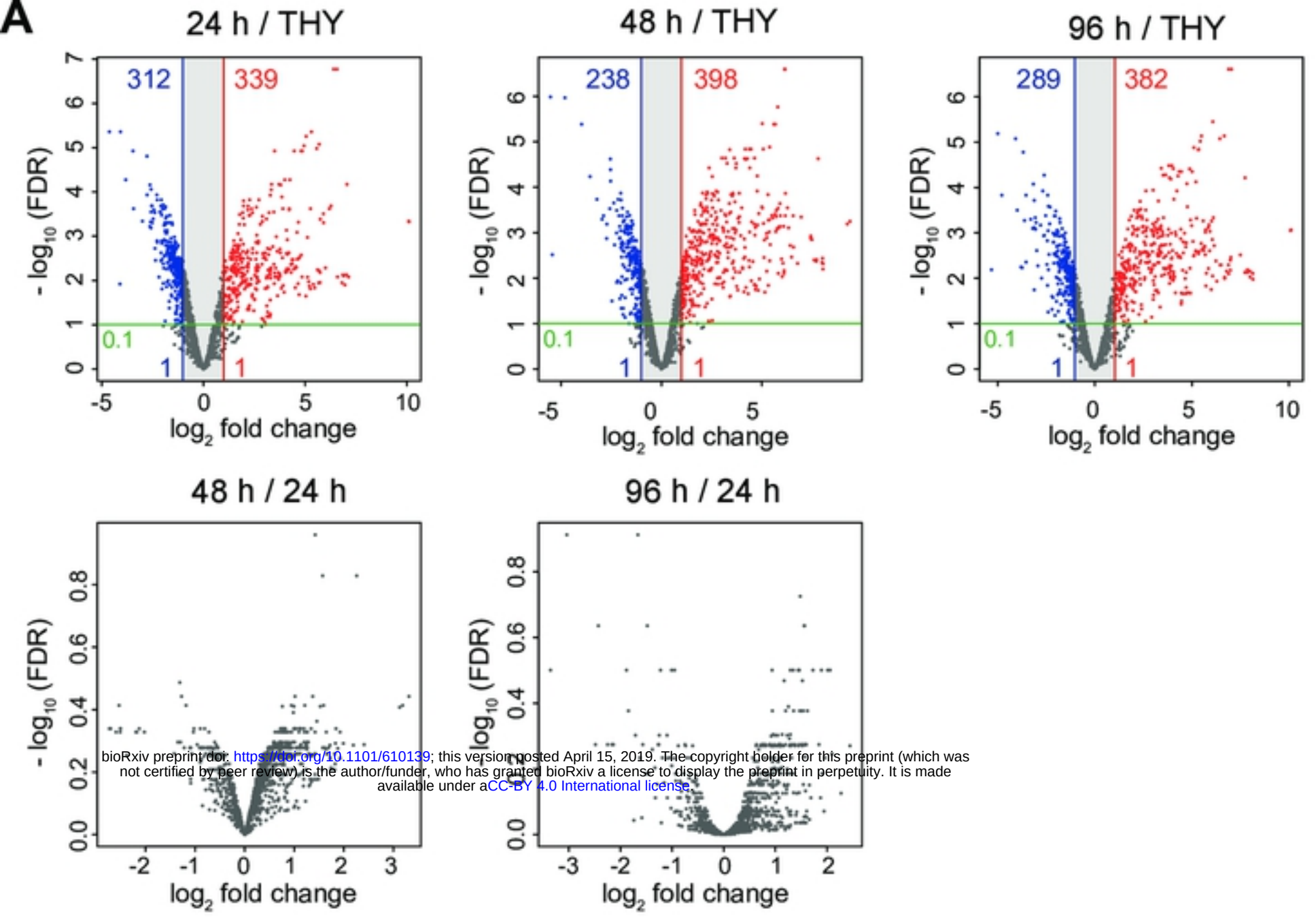

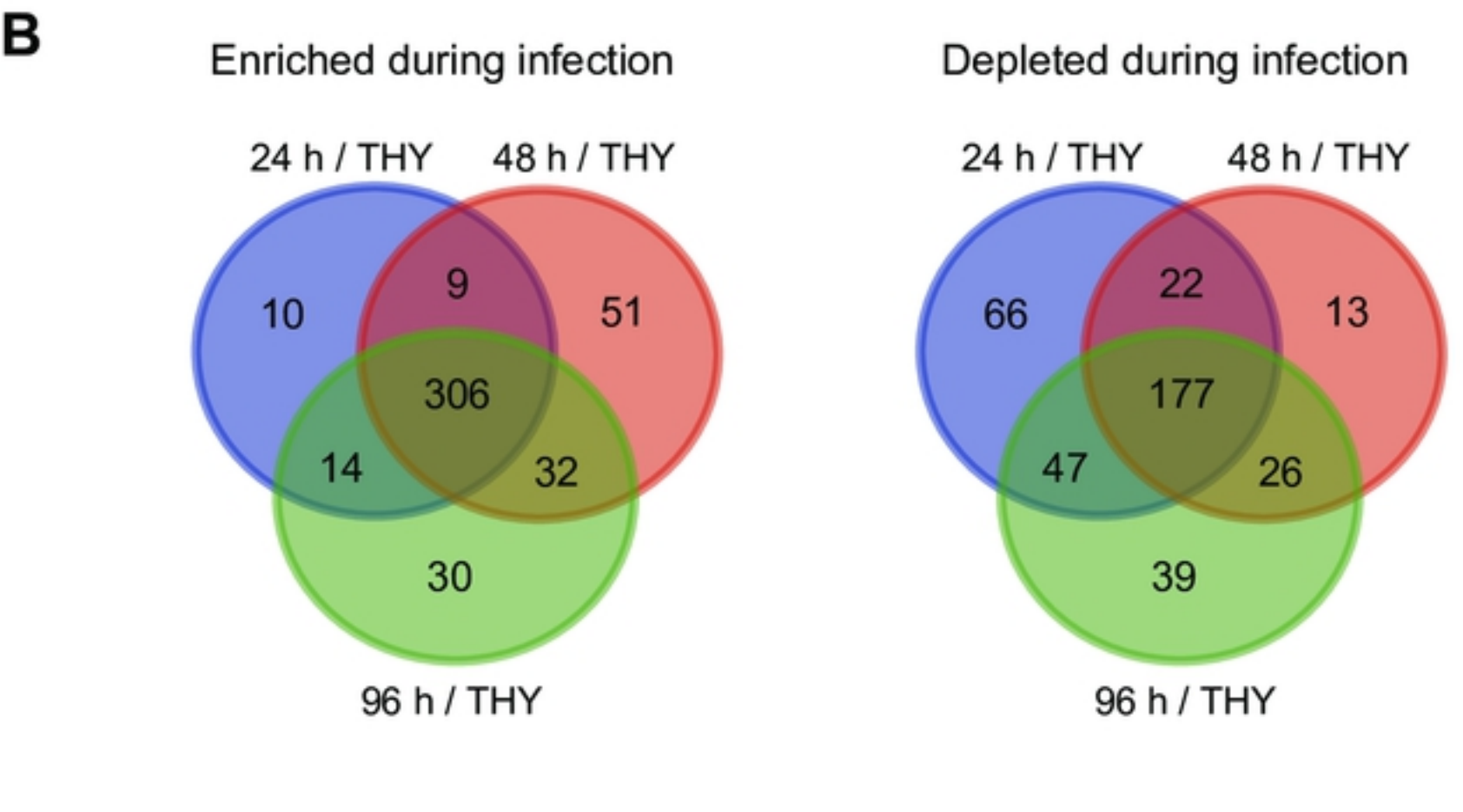

Figure 3. Hirose *et al.*

Figure 3

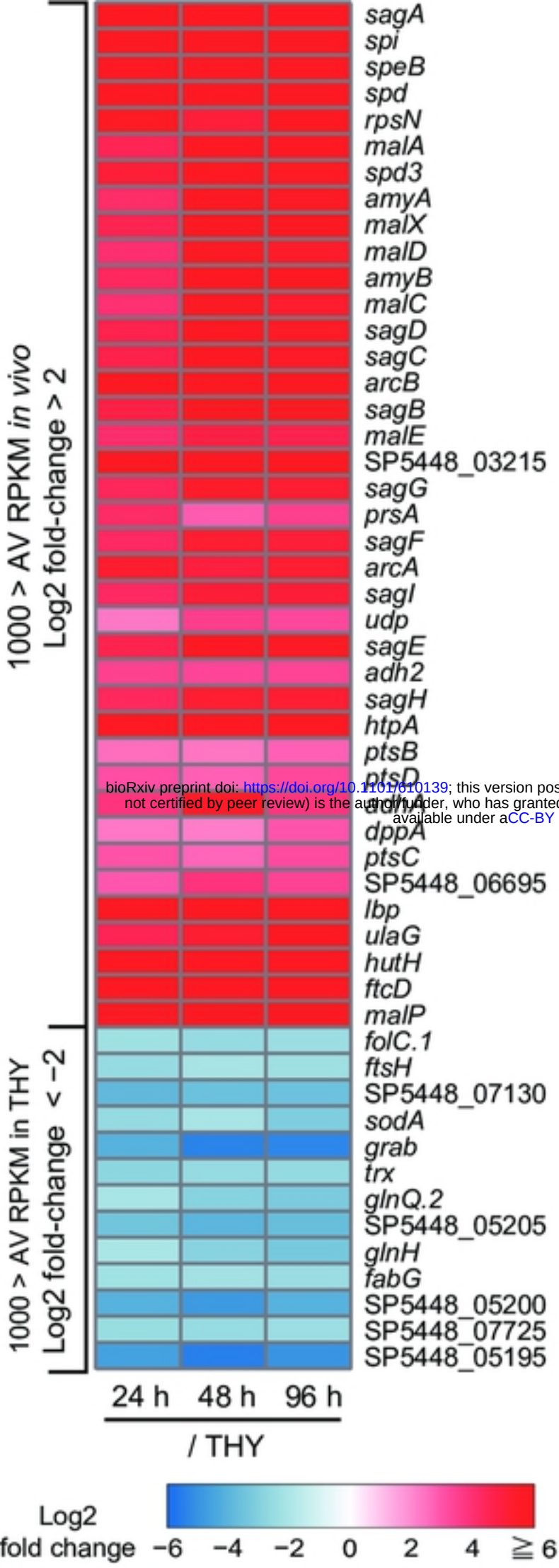

Figure 4. Hirose *et al.*

Figure 4

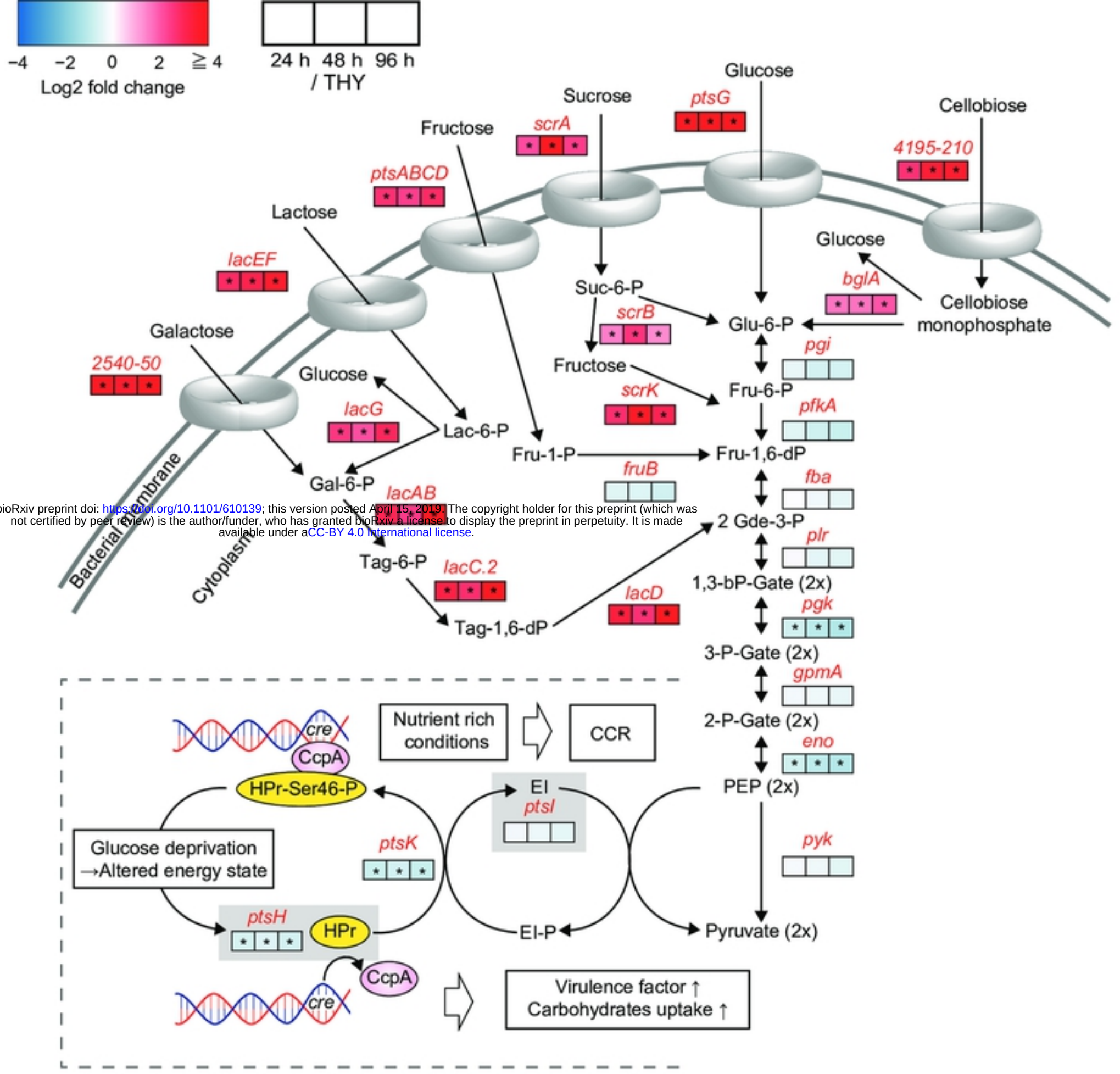

Figure 5. Hirose *et al.*

Figure 5

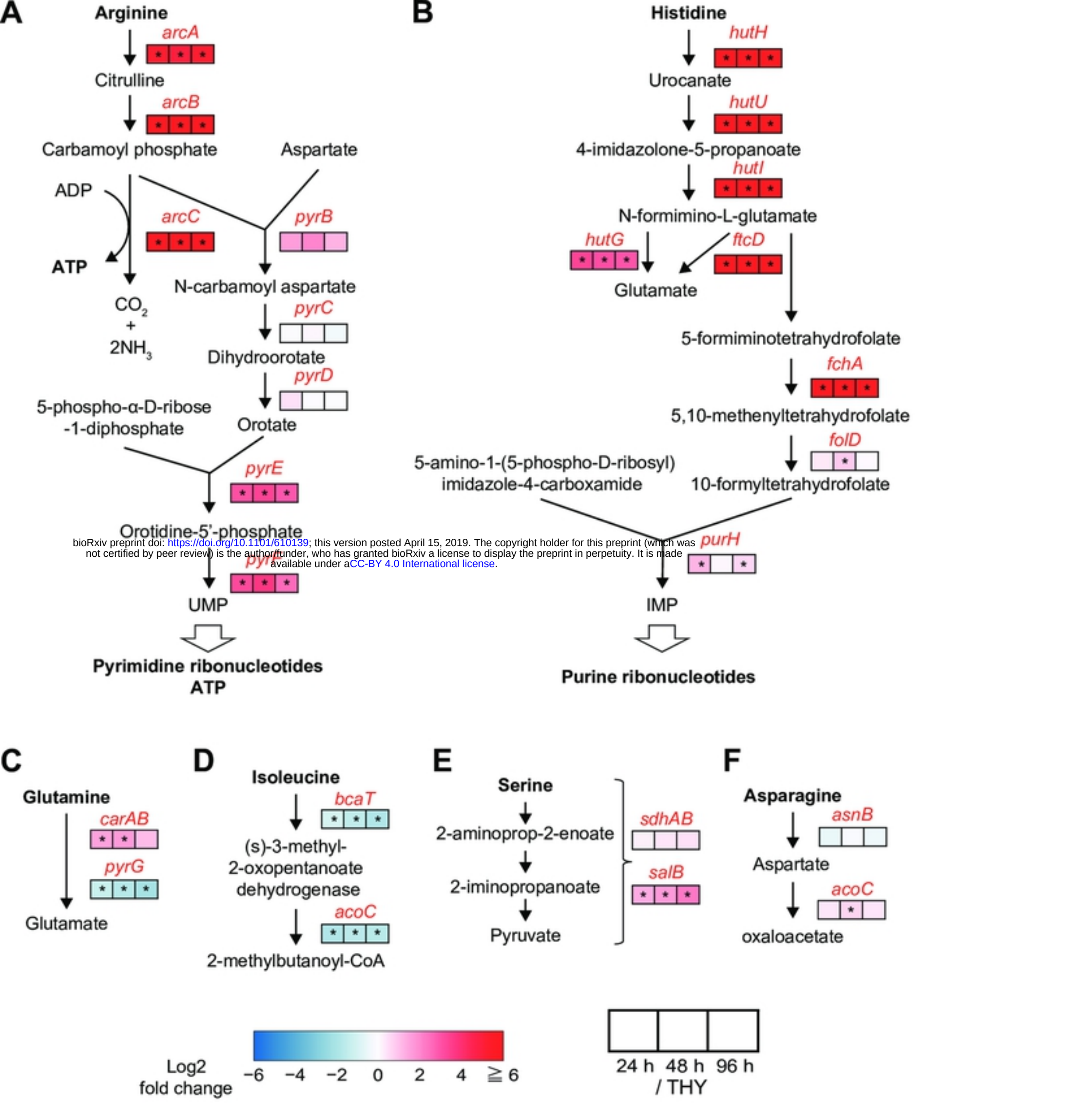

Figure 6. Hirose *et al.*

Figure 6

A TCS regulators of virulence

	24 h	48 h	96 h
trxR	3.69*	4.15*	4.06*
trxS	3.48*	4.03*	3.86*
sptS	0.25	0.34	0.28
sptR	-0.09	0.21	0.01
fasC	-0.33	-0.09	-0.19
fasA	-0.38	-0.06	-0.21
fasB	-0.45	-0.29	-0.82*
ciaH	-0.24	-0.11	-0.13
ciaR	-0.51	-0.31	-0.49
irr	-0.62*	-0.76*	-0.10
ihk	-0.68*	-0.74*	0.09
covR	-0.90*	-0.30	-0.92*
covS	-1.04*	-0.61*	-1.12*
vicR	-1.14*	-0.96*	-1.03*
vicK	-1.15*	-0.99*	-0.90*

/ THY

B Transcriptional regulators of virulence

	24 h	48 h	96 h
lacD.1	3.08*	2.80*	3.24*
rivR/ralp4	2.28*	2.73*	2.44*
malR	1.97*	2.05*	2.03*
ccpA	1.32*	1.56*	1.06*
mga	-0.12	0.22	0.81*
relA	-0.14	-0.35	-0.17
perR	-0.22	-0.26	-0.13
rgg	-0.22	-0.15	0.39
codY	-0.53	-0.18	-0.56
srv	-1.09*	-1.23*	-1.18*
mtsR/scaR	-1.32*	-0.86*	-1.65*
rofA	-1.41*	-0.76*	-0.69

/ THY

Log2 fold change

≧ 2
1
0
-1
−2

Consistently enriched and depleted genes

Figure 7. Hirose *et al.*

Figure 7

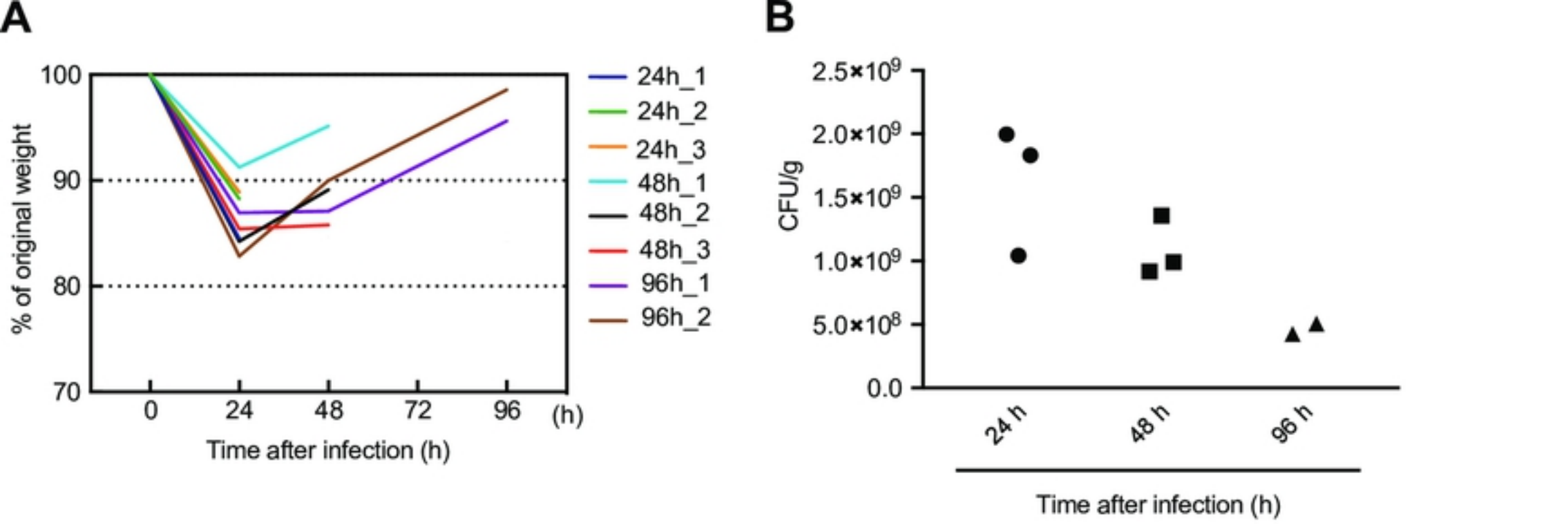

Supplementary figure 1. Hirose *et al.*

Supplementary Figure 1

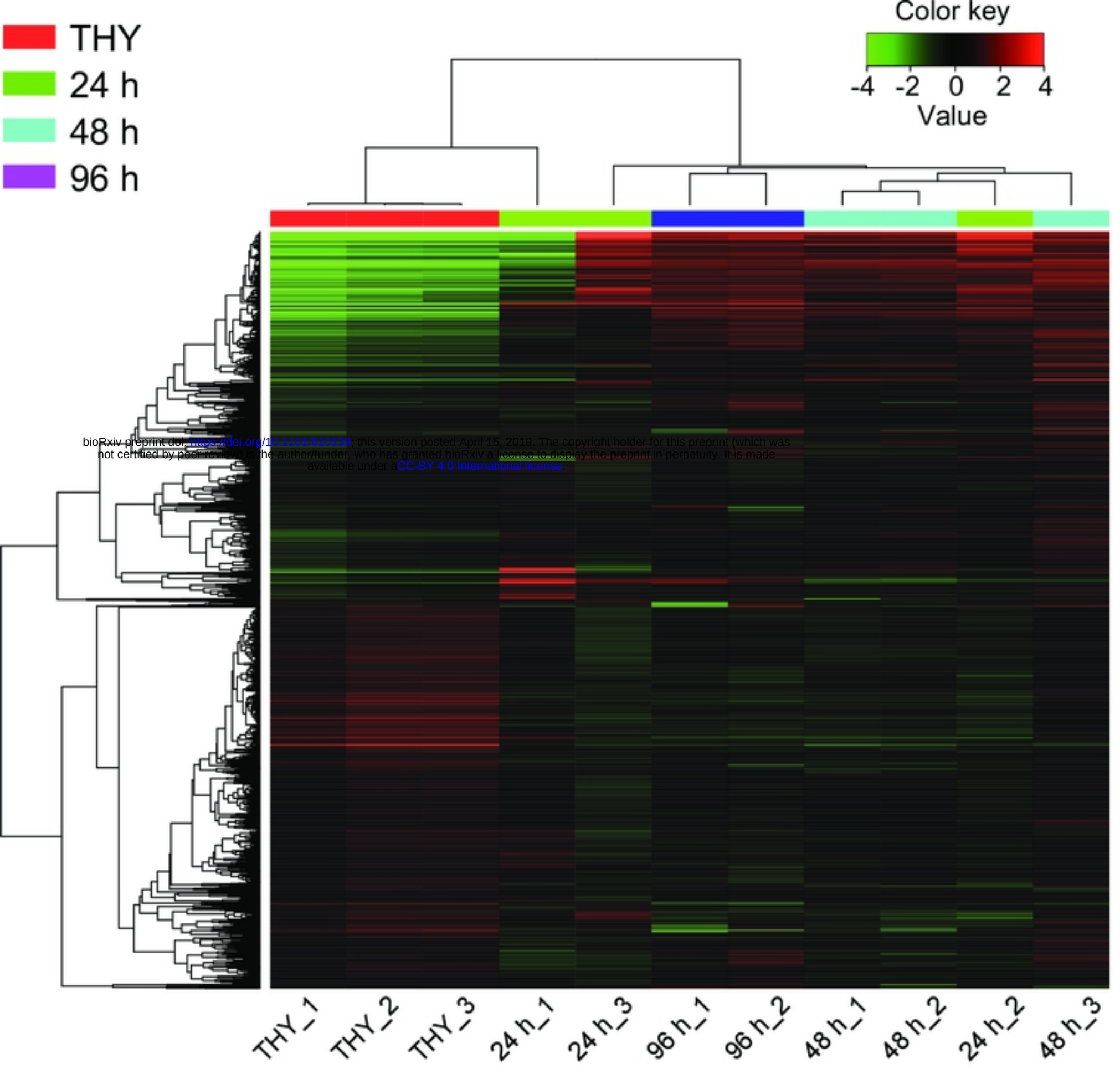

Supplementary figure 2. Hirose *et al.*

Supplementary Figure 2